In: Proceedings of 2013 Society of Experimental Mechanics Annual Conference, Paper 460, 2013.

Indentation Measurements on Soft Materials using Optical Surface Deformation Measurements

M.J. Wald
Graduate Research Assistant
University of Pennsylvania
220 S. 33rd St
Philadelphia, PA, USA, 19104-6315

J.M. Considine
Materials Research Engineer
US Forest Service, Forest Products Laboratory
One Gifford Pinchot Drive
Madison, WI, USA 53726

K.T. Turner
Associate Professor
University of Pennsylvania
220 S. 33rd St
Philadelphia, PA, USA, 19104-6315

ABSTRACT

Instrumented indentation is a common technique for measuring the elastic properties of bulk materials as well as thin films on substrates. However, in traditional indentation, it can be difficult to determine the true deformation of a specimen due to the effects of machine compliance and thermal drift. In the present work, a method is developed to track the in-plane and out-of-plane deformation of a specimen during indentation tests using fluorescent microparticles. Bead tracking and quantitative defocusing methods are used to track the in-plane and out-of plane displacements of the beads, respectively. Here, we describe the calibration of the system and assess the effects of particle size and magnification on the accuracy and resolution of the system. In addition, results from preliminary indentation tests performed on bulk polydimethylsiloxane specimens are reported. An analysis algorithm was developed to extract the elastic properties by measuring the displacements on the surface as a function of applied indentation force. Results are compared to traditional indentation measurements in which load and displacement are only measured at the indenter.

Keywords: Indentation, Soft Materials, Particle Tracking, Modulus, Poisson's Ratio

Introduction

Instrumented indentation is a common method for characterizing the mechanical properties of bulk materials. This technique is capable of testing small volumes of material at low loads and small displacements and allows for simple sample preparation compared to traditional tension or compression tests. Oliver and Pharr [1] describe a widely accepted method based on Sneddon's solution [2] for axisymmetric indentation of an elastic halfspace for determining a specimen's effective modulus ($E_{eff} = E/(1-\nu^2)$) from the measured applied load and displacement of the indenter. However, Young's modulus, E, and Poisson's ratio, ν, which are commonly used in engineering applications, cannot be independently determined using this analysis. To find E, it is necessary to guess or estimate ν, which is difficult to measure directly on small volumes of material with established techniques.

The Oliver-Pharr method is also affected by the sensitivity of measured stiffness to errors in the measurement of the true deformation of a specimen. These errors are commonly due to machine compliance and thermal drift. Machine compliance is commonly calculated by indenting a material with known elastic properties, such as fused silica, and subtracting the theoretical compliance of the material from the experimentally measured compliance [3, 4]. While this method provides an estimate for the machine compliance, it relies on an accurate measurement of the contact area and the ability to accurately detect the initial contact between the indenter and specimen, which is challenging when testing soft materials [5, 6]. Thermal drift, or the change in position of the sample relative to the indenter due to small changes in temperature, is often minimized by either conducting indentation tests in a closed environment in which the temperature is stable or performing indentation tests quickly [7].

In the present work, the displacement of the surface of the sample is measured independently of the indenter. Specifically, the displacement of fluorescent microparticles near the surface of the specimen during an indentation test are measured. In-plane motion is measured by tracking the particle center and out-of-plane motion is measured using the quantitative defocusing method. Measuring the displacement of the specimen surface at multiple locations in the vicinity of the indenter allows mechanics models that relate both in-plane and out-of-plane displacements to the applied load to extract elastic properties. The use of both in-plane and out-of-plane displacement permits both E and ν to be obtained. In addition, separating the displacement measurements from the indenter allows the deformation to be measured independently of machine compliance and drift.

The purpose of the present work is to assess the accuracy and precision of the in-plane and out-of-plane displacement measurements using particle tracking and quantitative defocusing, respectively. The accuracy of these techniques depend on experimental conditions including optical properties of the microscope and specimen, thus the effect of magnification and particle size on the accuracy and resolution of the technique are investigated for particles on PDMS. Preliminary cylindrical flat punch indentation tests are performed on PDMS specimens and the in-plane and out-of-plane displacements are used along with load data to identify E and ν. These results are compared with E_{eff} calculated using standard indentation analysis.

Background

Instrumented Indentation

Instrumented indentation is a frequently used technique for evaluating mechanical properties of soft materials, including polymers and biological tissues [8]. This method is capable of testing at low loads and displacements and sample preparation is simple compared to traditional tension or compression tests. Here, we consider flat punch indentation in which a force, P, is applied to a cylindrical flat punch with radius, a, indenting it into an elastic halfspace with Young's modulus, E, and Poisson's ratio, ν. The origin of the Cartesian coordinate system used in the present work is located on the surface of the specimen and along the centerline of the indenter. z is positive into the material, such that a compressive force deforms the specimen in the positive z direction. For rigid cylindrical flat punch indentation, E_{eff} relates to the stiffness measured during an indentation test as follows [1, 2]:

$$E_{eff} = \frac{E}{1-\nu^2} = \frac{k}{2a}, \tag{1}$$

where E is the Young's modulus, ν is the Poisson's ratio, k is the stiffness, and a is the contact radius.

The in-plane and out-of-plane displacements of a point on the surface of an elastic halfspace that is being indented with a cylindrical flat punch are a function of E, ν, a, in-plane position, x and y, and applied load, P [9]. The

relationships were transformed to Cartesian coordinates to better facilitate experimental data from the camera. Beneath the indenter, the displacements are

$$
\begin{aligned}
u_x &= -\frac{(1-2\nu)(1+\nu)}{2\pi E}\frac{Px}{x^2+y^2}\left(1-\sqrt{1-\frac{x^2+y^2}{a^2}}\right) \\
u_y &= -\frac{(1-2\nu)(1+\nu)}{2\pi E}\frac{Py}{x^2+y^2}\left(1-\sqrt{1-\frac{x^2+y^2}{a^2}}\right) \\
u_z &= \frac{1-\nu^2}{\pi E}\frac{P}{a}
\end{aligned}
\tag{2}
$$

and outside the contact area,

$$
\begin{aligned}
u_x &= -\frac{(1-2\nu)(1+\nu)}{2\pi E}\frac{Px}{x^2+y^2} \\
u_y &= -\frac{(1-2\nu)(1+\nu)}{2\pi E}\frac{Py}{x^2+y^2} \\
u_z &= \frac{1-\nu^2}{\pi E}\frac{P}{a}\arcsin\left(\frac{a}{\sqrt{x^2+y^2}}\right).
\end{aligned}
\tag{3}
$$

Quantitative Defocusing Method

Discrete micrometer-scale particles are widely used as markers to measure displacements in both fluids and soft solids, including gels and biological materials [10]. Scanning confocal microscopy is a popular tool for quantifying the position of micrometer-scale particles in three dimensional space because the spatial resolution is superior to many other techniques [11]. However, because scanning confocal microscopes scan the specimen point by point, the data acquisition rates are generally slow [12], which becomes problematic when high acquisition rates are required to quantify time-dependent material properties.

An alternative method called quantitative defocusing [13], has lower resolution than scanning confocal microscopy, but can achieve higher acquisition rates. This method uses wide-field fluorescence microscopy to image micron-scale fluorescent particles. Unlike confocal microscopy which restricts out-of-focus light, in wide-field microscopy, out-of-focus particles appear along with particles in the focal plane. Due to spherical lens aberration, a ring pattern forms around the out-of-focus particles. The radius of the ring is a function of the distance of the particle from the focal plane [13, 14]. This method is advantageous because the entire field-of-view is captured in one image, allowing for data acquisition rates faster than conventional confocal microscopy. In addition, wide-field fluorescence microscopes are often less expensive than confocal microscopes.

Non-ideal optical conditions typically limit the use of diffraction models, thus a commonly used approach is to compare the aberration rings measured during experiments to an experimentally developed calibration curve. The calibration curve is created by collecting images of a stationary particle of the same size as those used in the experiment at known z displacements from the focal plane. The ring shape is measured to correlate ring size with out-of-plane displacement [15]. While the calibration curve depends on the objective, particle size, and the optical properties of the system and cannot be used universally, this method allows displacement to be measured in situations in which the optical properties of the system are not ideal. Zhang and Menq [16] developed a method in which the in-plane location of a particle is found using a weighted centroid method. The intensity of the particle and ring aberration is found as a function of radial distance from the centroid. This intensity profile is compared to those of calibration images to determine the out-of-plane displacement. Using this analysis technique with 4.5 μm particles and a magnification of 60x, an in-plane standard deviation of 0.35 nm and an out-of-plane standard deviation of 0.9 nm was reported. Because applying quantitative defocusing to indentation tests requires viewing the particles through the specimen, which can be several millimeters thick, a similar approach in which calibration curves are created experimentally prior to testing is pursued in the present work.

Experimental Setup

PDMS is prepared by mixing a 10:1 weight ratio of Sylgard 184 base elastomer to Sylgard 184 curing agent (Dow Corning Corporation, Midland, MI). After degassing for 1 hr, the PDMS is cast on a silicon wafer to ensure a smooth surface for indentation. The PDMS is cured on a hot plate at 85° C for 4 hr. Fluorescent polystyrene microspheres (Bangs Laboratories, Inc, Fishers, IN) are used for surface motion markers. The microspheres have an excitation wavelength of 480 nm and an emission wavelength of 520 nm. 1 μL of microbead solution is diluted in 1 mL of isopropanol. This bead mixture was placed on the surface of PDMS in 1.5 μL drops. Specimens were allowed to sit for at least 12 hrs to ensure the isopropanol had completely evaporated.

A cylindrical flat punch indentation experiment was developed to validate the technique proposed in this work. A wide-field fluorescence inverted microscope was built to image the particles from beneath the specimen during indentation tests. Images were collected from the microscope with a CMOS (1024 x 1280) camera (Pixelink A741, Ottawa, Ontario). The specimen is placed on a closed-loop nanopositioning stage (nPoint, Middleton, WI) which has a 100 μm in-plane and out-of-plane displacement range. To facilitate the inverted microscope, the stage has an opening in the center, giving the microscope access to the specimen. This stage is mounted on a tip-tilt stage to allow proper alignment between the sample and the indenter. A schematic of the experiment setup is shown in Figure 1. The cylindrical flat punch indenter is made from a 0.5 mm diameter glass rod. Force is measured with a 10 g load cell (Cooper Instruments and Systems, Warrenton, VA).

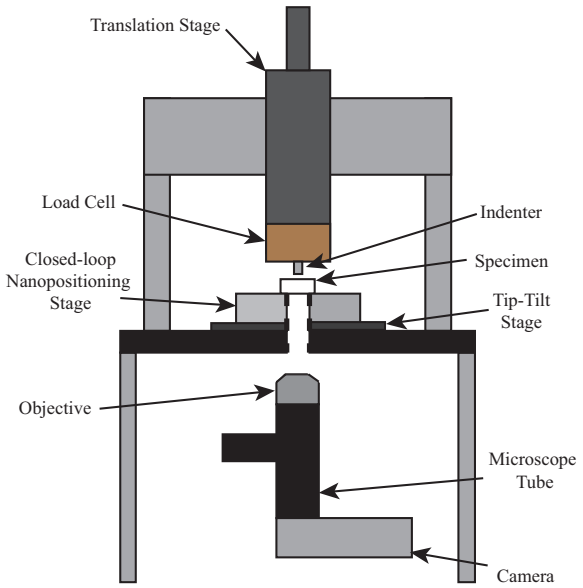

Figure 1: Schematic of the indenter. A translation stage moves the load cell and indenter into and out of contact with the specimen which is mounted over an opening. The opening allows the inverted microscope to view the displacement of the microparticles during the indentation test.

Particle Tracking Procedure

In the present work, the x coordinate was defined in the 1280 pixel direction of the camera and the y coordinate was defined along the 1024 pixel direction. Preprocessing consists of background subtraction, image contrast adjustment, and median filtering. The background image is created by averaging 5 images of the specimen taken at a sufficient distance from the focal plane such that the particles are not identifiable from the background. The image contrast is adjusted to increase the brightness of the particles relative to the background noise. Lastly, a 3x3 median filter is applied to remove salt and pepper noise.

To identify peaks, the first image in an image sequence is converted to binary. Bright regions are then identified as potential particle locations. These are then filtered based on area and minimum peak height to exclude areas not associated with particles. Minimum area, maximum area, and peak height are adjustable parameters meant to allow

the user to sort out particles of interest from surface contamination or noise that may not have been removed during image preprocessing.

The particles that meet these criteria are located in the grayscale image and fit with the first 30 axisymmetric Zernike polynomials. While the definition of Zernike polynomials is beyond the scope of this work, additional information can be found here [17]. Zernike polynomials were chosen because the axisymmetric mode shapes resemble the intensity distribution of both in-focus and out-of-focus fluorescent particles. A bounding box around each particle is created. The center of a bounding box created around a particle, which corresponds to the origin of the axisymmetric Zernike polynomials, is allowed to vary to minimize the error between the axisymmetric Zernike polynomial fit and the grayscale values inside the bounding box. If the error is below a threshold value set by the user, the region is considered a valid particle. The center of the bounding boxes of valid particles are then used as initial guesses for the in-plane particle locations in all images. These regions are then fit in each image using the Zernike polynomial algorithm to determine the particle centers.

To determine the out-of-plane location of the particles, the intensity of the Zernike polynomial fits for each particle are normalized such that the peak is 1. The ring radius of the particle is determined by finding the radius of the smallest circle that will enclose the points on the Zernike polynomial in which the height is greater than or equal to 0.5. This threshold was chosen because it exceeds the noise in the fitted surface that sometimes appears along the boundaries of the bounding box.

Calibration

Procedure

To understand the effects of particle size and magnification on the accuracy and precision of displacement measurements, displacement calibration and noise data were collected for 1.9 μm and 6.3 μm diameter particles on a 3 mm thick PDMS sample using a 10x Zeiss EC Epiplan-Neofluar objective with a 9 mm working distance and 0.25 numerical aperture and a 20x Zeiss LD EC Epiplan-Neofluar objective with a 12.1 mm working distance and 0.22 numerical aperture. These objectives were chosen because the relatively long working distance is necessary to view the particles through thick specimens. For thin specimens, an objective with a shorter working distance would be advantageous because it would have a higher numerical aperture, which increases the light intensity of the particles and decrease the depth of field. In-plane displacements are calibrated by translating an undeformed specimen with the piezoelectric stage in the stage's x, y, and z directions and measuring the motion of the particle center and radius. For z calibration the specimen is translated 100 μm in 1 μm increments. For both x and y directions, the specimen is moved 5μm in 0.1 μm increments. After each step, the stage is allowed to settle for 1 second, at which point an image is captured.

Results

Figure 2 shows 1.9 μm and 6.3 μm particles at 10x and 20x at different distances from the focal plane. For the cases shown, as the particle moves out of focus, the observed area increases and the observed intensity decreases. Because of this effect, it is necessary to choose a particle size that will allow the particle to be seen over the desired out-of-plane displacement range. At a 20x magnification, the 1.9 μm particle is not visible at 20 μm or 40 μm. The 1.9 μm particle at 10x magnification begins to fade after moving more than 20 μm from the focal plane.

It is possible to increase the out-of-plane range of this method by using an objective with a higher numerical aperture or increasing light intensity [13]. While the long working distance needed to view the particles through a specimen limits the numerical aperture that can be used, the light intensity can be increased by using larger particles. As shown in Figure 2, at both magnifications, the 6.3 μm particles have a higher intensity and the edge of the bead is better defined than than the 1.9 μm beads at the off-focus distances examined.

Figure 3 shows the relationship between the change in measured radius relative to the in-focus particle radius and distance from the focal plane for three 1.9 μm and 6.3 μm particles with the 10x objective. The radius of the 1.9 μm particles are shown from 0 to 30 μm away from the focal plane in Figure 3a. Beyond this distance, the algorithm was unable to distinguish the particles from the background noise. In Figure 3b, the algorithm was able to track the particle radius from 0 to 100 μm from the focal plane. The discontinuities in the measured change in radius that occur between stage displacements of 50 μm to 70 μm are currently being investigated. These results suggest that

6.3 μm particles are better suited for these experimental conditions because the increase in light intensity allows them to be identified and tracked farther from the focal plane.

The in-plane motion of 1.9 μm and 6.3 μm particles were calibrated with the respect to the displacement of the stage for magnifications of 10x and 20x. The results of x and y calibrations for 6.3 μm particles at 10x and 20x magnification are shown in Figure 4. As expected, the in-plane displacement of the particles are linearly related to the applied displacement from the piezoelectric stage. The slope of the pixel displacement - stage displacement relationship was found using linear least squares.

The mean and standard deviation of the slopes for all particles tracked for each case are shown in Table 1. The mean slopes agree reasonably well with an independent microscope calibration which used a 0.02 mm optical calibration standard. For the 10x objective, the x calibration was 613 nm/pixel and the y calibration was 612 nm/pixel. Using the 20x objective, the x calibration is 303 nm/pixel and the y calibration is 305 nm/pixel.

Table 1: Mean and standard deviation x and y calibration relationships for all particles at 10x and 20x magnification

	x calibration		y calibration	
	Mean (nm/pixel)	Std Dev (nm/pixel)	Mean (nm/pixel)	Std Dev (nm/pixel)
1.9 μm particle, Mag. 10x	576	183	548	184
1.9 μm particle, Mag. 20x	307	13	311	4
6.3 μm particle, Mag. 10x	606	4	637	26
6.3 μm particle, Mag. 20x	316	2	294	3

Uncertainty Measurement

Procedure

To quantify the in-plane noise in the image analysis, 50 images were collected for a stationary specimen over a period of 128 seconds. Using the algorithm described previously, the center of each particle is tracked in each image. The motion of the particle center can then be correlated with the displacement of stage.

Results

A summary of the mean and standard deviation of the measured in-plane displacements for magnifications of 10x and 20x and particle sizes of 1.9 μm and 6.3 μm are shown in Table 2. The nonzero mean values may be due to drift in the sample. The standard deviations show that for both particle sizes, the 20x objective has a higher precision. This suggests that there is a trade-off between precision of the in-plane measurement and the field-of-view of the experiment.

Indentation Experiments

Experimental Procedure

Preliminary indentation tests on a PDMS specimen with 6.3 μm beads on the surface was completed using the indentation system described previously fitted with a 20x objective. The piezoelectric stage was initially moved to 15 μm above the focal plane. The indenter was positioned such that it was within a few micrometers, but not in contact, with the specimen. The stage is then moved 40 μm toward the indenter over 10 s. The maximum stage displacement is then held for 10 s. The stage was then moved -55 μm. The additional unloading displacement is added to account for adhesion between the indenter and specimen. The measured stiffness is calculated by fitting the unloading portion of the force-displacement data from 90% of the maximum compressive load to 10% of the maximum compressive load with a linear relationship and calculating the slope.

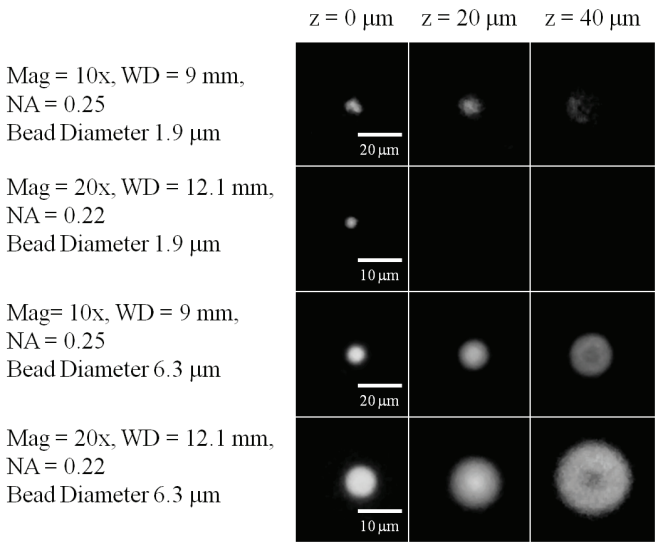

Figure 2: 1.9 μm and 6.3 μm diameter polystyrene fluorescent particles shown at 10x and 20x magnification at 0 μm, 20 μm, and 40 μm from the focal plane.

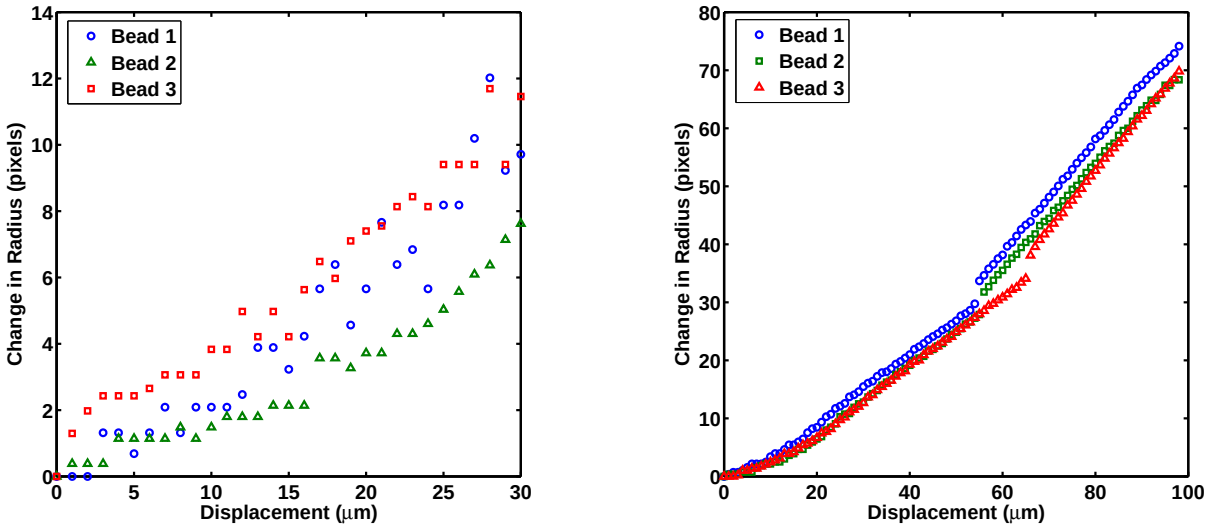

(a) (b)

Figure 3: Change in radius of the particle as a function of out-of-plane displacement for a 10x objective and a) 1.9 μm diameter particles and b) 6.3 μm diameter particles.

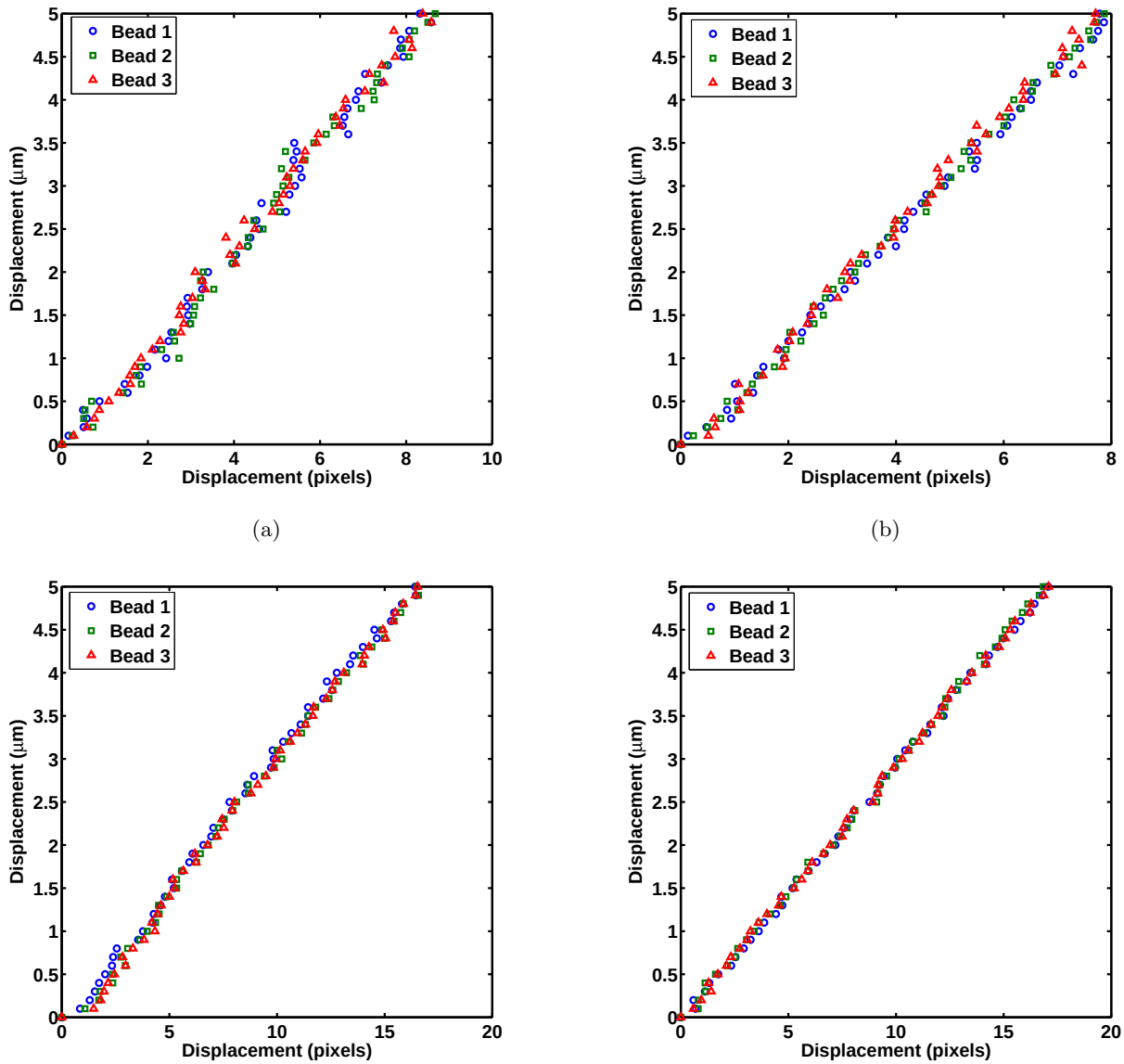

(a) (b) (c) (d)

Figure 4: a)10x magnification x calibration, b) 10x magnification y calibration, c) 20x magnification x calibration, and d) 20x magnification y calibration for 6.3 μm particles.

Table 2: Mean and standard deviation x and y noise measurements for all particles at 10x and 20x magnification

	x displacement		y displacement	
	Mean (nm)	Std Dev (nm)	Mean (nm)	Std Dev (nm)
1.9 μm particle, Mag. 10x	125	232	-37	201
1.9 μm particle, Mag. 20x	-237	82	-0.25	76
6.3 μm particle, Mag. 10x	-242	248	-232	294
6.3 μm particle, Mag. 20x	-166	91	17	65

Analysis

An optimization routine was developed to extract E and ν from displacement data for discrete particles. This model requires in-plane positions of the particles, x, y, and z displacements at the particle locations, the measured force, and the indenter radius to be known. E and ν are found using a nonlinear least squares algorithm, which varies E and ν to minimize the error between experimental displacement data and theoretical displacements calculated from eqs. 2 and 3. The identification of E and ν has not been optimized to reduce the effect of noise on the displacement measurements. This will be addressed in future work.

To validate the results from the optimization routine, E_{eff} is calculated using the Oliver and Pharr method [1] using stage displacement and load cell measurements. To calculate the specimen stiffness, it is necessary to account for machine compliance. Following the method proposed by Oliver and Pharr [1], the measured compliance is modeled as two springs combined in series as follows:

$$C_{measured} = C_{specimen} + C_{machine}, \tag{4}$$

where $C_{measured}$, $C_{specimen}$, and $C_{machine}$ are the measured compliance, specimen compliance, and machine compliance respectively. For flat punch indentation, $C_{specimen}$ is

$$C_{specimen} = \frac{1}{2E_{eff}a}. \tag{5}$$

$C_{machine}$ was determined using a 6.35 mm thick fused silica specimen (E = 72 GPa, ν=0.17 [1]). Using the fused silica properties and $C_{measured}$ from 11 indentation tests in eq. 4, the mean $C_{machine}$ is 880 μm/N with a standard deviation of 4.76 μm/N. The large compliance in the system is predominately due to the compliance of the 10g load cell. Because $C_{machine}$ is a property of the instrument, it can be used along with $C_{measured}$ from indentation tests in eq. 4 to find $C_{specimen}$ for materials with unknown properties. The effective modulus can then be calculated from eq. 5.

Results

Images of the particles outside the contact area from the experiment are shown in Figure 5. Figure 5a show the particles when they are 15 μm away from the focal plane and the indenter is not in contact with the specimen. In Figure 5b, the specimen is moved 40 μm from it's initial position. As expected, the radius of all particles except particle 2 increase. It is not understood why particle 2 does not appear in Figure 5b. The out-of-plane calibration was completed by fitting a 6th order polynomial to out-of-plane calibration data taken for these particles over a stage displacement range of 0 to 55 μm, which corresponds with the displacement range of the experiment. Because the polynomial fit does not describe the relationship between particle radius and stage displacement well for particles 1 and 6, only data from particles 3, 4, and 5 are included in this analysis. Stage displacement and measured bead displacement of particles 3, 4 and 5 are shown in Figure 6a and the measured load corresponding to each image is shown in Figure 6b. The surface deformation, which is needed for the analysis, is the difference between stage displacement and particle displacement at a given time.

Force measurements, indenter radius, in-plane particle location, and x, y, and z particle displacements measured from images captured when the stage was at the maximum displacement were input into the analysis algorithm and E and ν were calculated for each image. ν was bounded between 0 and 0.5. E and ν were determined to be 1.98 $\pm$ 0.16 MPa and 0.5 respectively, leading to an E_{eff} of 2.64 $\pm$ 0.21 MPa. While PDMS is expected to have a Poisson's ratio near 0.5, the algorithm may be reaching the upper bound due to errors in the in-plane measurements. For comparison, E_{eff} was calculated from the compliance measured during the unloading portion of the force-displacement relationship. After correcting for machine compliance, E_{eff} is 3.23 MPa. While the particle tracking analysis and the traditional analysis do not agree, they are similar. Errors in the measured machine compliance effect the modulus calculated using the traditional analysis. There are also sources of error in the bead tracking technique. While the analytical model assumes the contact between the indenter and specimen is frictionless, there are friction and adhesive effects that may be influencing the in-plane displacements. Only three particles were tracked in the present work. A previous numerical study of this system suggested that at least 36 particles are required to find E and ν within $\pm$5% of the true value [18]. Future work includes addressing the in-plane measurement errors and increasing the particle density to improve the accuracy and precision of E and ν calculated from the particle tracking method.

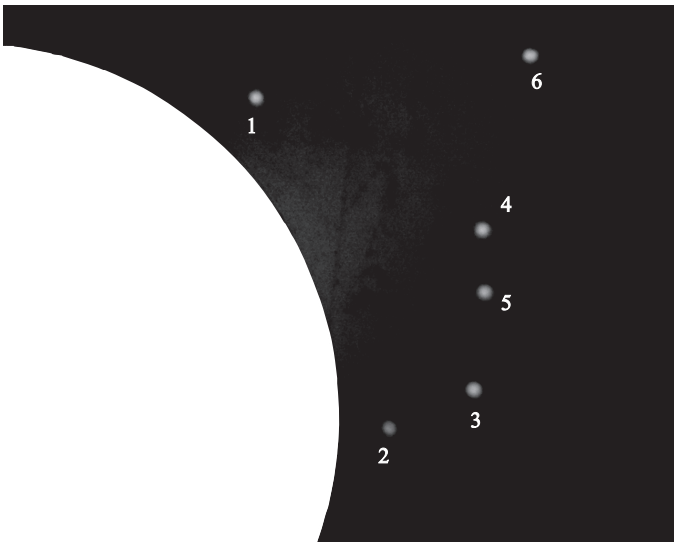

(a)

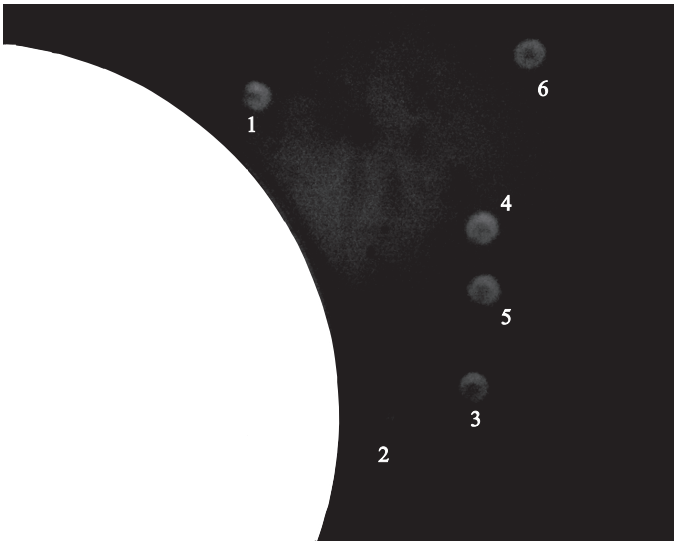

(b)

Figure 5: Images of beads outside of the contact region from the experiment a) 15 μm out-of-focus b) 55 μm out-of-focus. The white region is the portion of the contact region visible during the experiment

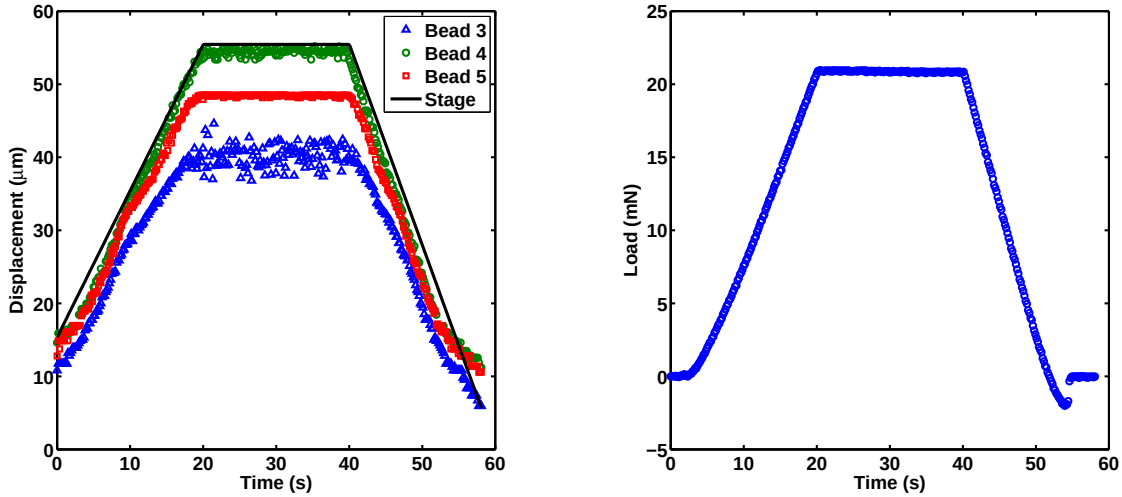

(a) (b)

Figure 6: a) The measured out-of-plane displacement as a function of time for an indentation test on PDMS. Data points show the out-of-plane displacement in each image as a function of time. The solid line in a) shows the displacement of the stage. The displacement of the surface at the particle locations is the difference between the stage displacement and measured bead location. b) The measured load corresponding to each image as a function of time.

Conclusion

A technique for measuring the in-plane and out-of-plane displacements along the surface of a transparent specimen during a flat punch indentation test was designed. An algorithm was developed to track the in-plane and out-of-plane motion of discrete particles by fitting images of the particles with axisymmetric Zernike polynomials. The viability of this method was assessed by applying the algorithm to in-plane and out-of-plane calibrations and in-plane noise measurement of fluorescent particles on PDMS. For the optical system used in the present work, it was found that 6.3 μm particles provide sufficient light intensity to be tracked over 100 μm of out-of-plane displacement. The noise assessment suggests that the precision of the in-plane measurements improved at higher magnification. However, as the field-of-view decreases, less particles can be tracked, which may affect the performance of the analysis algorithm. A preliminary indentation test was completed to demonstrate the feasibility of the technique. An optimization routine was used to extract E and ν from load, particle location, particle displacement, and contact radius data. Discrepancies between E_{eff} calculated from the particle tracking method and the Oliver and Pharr method may be due to errors in machine compliance measurements, having insufficient particles within the field-of-view, and friction and adhesive effects not accounted for in the analytical model. These errors will be investigated in the future.

Acknowledgments

We wish to acknowledge financial support from the US Postal Service and US Forest Service, Forest Products Laboratory.

References

[1] W. C. Oliver and G. M. Pharr, "An improved technique for determining hardness and elastic-modulus using load and displacement sensing indentation experiments," *Journal of Materials Research*, vol. 7, no. 6, pp. 1564–1583, 1992.

[2] I. N. Sneddon, "The relation between load and penetration in the axisymmetric Boussinesq problem for a punch of arbitrary profile," *International Journal of Engineering Science*, vol. 3, no. 1, pp. 47–57, 1965.

[3] M. R. VanLandingham, "Review of instrumented indentation," *Journal of Research of the National Institute of Standards and Technology*, vol. 108, no. 4, pp. 249–265, 2003.

[4] A. Fischer-Cripps, "Critical review of analysis and interpretation of nanoindentation test data," *Surface and Coatings Technology*, vol. 200, pp. 4153–4165, Apr. 2006.

[5] M. J. Wald, J. M. Considine, and K. T. Turner, "Determining the elastic modulus of compliant thin films supported on substrates from flat punch indentation measurements," *Experimental Mechanics*, 2013, doi: 10.1007/s11340-012-9705-2.

[6] J. D. Kaufman and C. M. Klapperich, "Surface detection errors cause overestimation of the modulus in nanoindentation on soft materials," *Journal of the Mechanical Behavior of Biomedical Materials*, vol. 2, pp. 312–317, Aug. 2009.

[7] J. Nohava, N. X. Randall, and N. Conté, "Novel ultra nanoindentation method with extremely low thermal drift: principle and experimental results," *Journal of Materials Research*, vol. 24, no. 03, pp. 873–882, 2009.

[8] M. Oyen, "Nanoindentation of Biological and Biomimetic Materials," *Experimental Techniques*, vol. 37, no. 1, pp. 73–87, 2013.

[9] D. Maugis, *Contact, Adhesion and Rupture of Elastic Solids.* Berlin: Springer, 1 ed., 2000.

[10] S. S. Rogers, T. A. Waigh, X. Zhao, and J. R. Lu, "Precise particle tracking against a complicated background: polynomial fitting with Gaussian weight," *Physical Biology*, vol. 4, pp. 220–227, Oct. 2007.

[11] V. Prasad, D. Semwogerere, and E. R. Weeks, "Confocal microscopy of colloids," *Journal of Physics: Condensed Matter*, vol. 19, p. 113102, Mar. 2007.

[12] D. Semwogerere and E. R. Weeks, "Confocal microscopy," in *Encyclopedia of Biomaterials and Biomedical Engineering*, pp. 1–10, Taylor & Francis, 2005.

[13] M. Wu, J. W. Roberts, and M. Buckley, "Three-dimensional fluorescent particle tracking at micron-scale using a single camera," *Experiments in Fluids*, vol. 38, pp. 461–465, Feb. 2005.

[14] S. J. Williams, C. Park, and S. T. Wereley, "Advances and applications on microfluidic velocimetry techniques," *Microfluidics and Nanofluidics*, vol. 8, pp. 709–726, Mar. 2010.

[15] S. D. Peterson, H.-S. Chuang, and S. T. Wereley, "Three-dimensional particle tracking using micro-particle image velocimetry hardware," *Measurement Science and Technology*, vol. 19, p. 115406, Nov. 2008.

[16] Z. Zhang and C.-H. Menq, "Three-dimensional particle tracking with subnanometer resolution using off-focus images," *Applied Optics*, vol. 47, p. 2361, Apr. 2008.

[17] V. N. Mahajan, "Zernike circle polynomials and optical aberrations of systems with circular pupils," *Applied Optics*, vol. 33, no. 34, pp. 8121–8124, 1994.

[18] M. J. Wald, J. M. Considine, and K. T. Turner, "Improved instrumented indentation of soft materials through surface deformation measurements," in *Mechanics of Biological Systems*, vol. 5, pp. 141–147, 2013.